Analyst

ROYAL SOCIETY OF CHEMISTRY

PAPER

View Article Online
View Journal | View Issue

Cite this: *Analyst*, 2020, **145**, 4852

Dynamic single-cell intracellular pH sensing using a SERS-active nanopipette†

Jing Guo,[a] Alberto Sesena Rubfiaro,[a] Yanhao Lai,[b] Joseph Moscoso,[a] Feng Chen,[a] Yuan Liu,[b,c] Xuewen Wang [a] and Jin He *[a,c]

Received 26th April 2020,
Accepted 13th May 2020

DOI: 10.1039/d0an00838a

rsc.li/analyst

Glass nanopipettes have shown promise for applications in single-cell manipulation, analysis, and imaging. In recent years, plasmonic nanopipettes have been developed to enable surface-enhanced Raman spectroscopy (SERS) measurements for single-cell analysis. In this work, we developed a SERS-active nanopipette that can be used to perform long-term and reliable intracellular analysis of single living cells with minimal damage, which is achieved by optimizing the nanopipette geometry and the surface density of the gold nanoparticle (AuNP) layer at the nanopipette tip. To demonstrate its ability in single-cell analysis, we used the nanopipette for intracellular pH sensing. Intracellular pH (pH_i) is vital to cells as it influences cell function and behavior and pathological conditions. The pH sensitivity was realized by simply modifying the AuNP layer with the pH reporter molecule 4-mercaptobenzoic acid. With a response time of less than 5 seconds, the pH sensing range is from 6.0 to 8.0 and the maximum sensitivity is 0.2 pH units. We monitored the pH_i change of individual HeLa and fibroblast cells, triggered by the extracellular pH (pH_e) change. The HeLa cancer cells can better resist pH_e change and adapt to the weak acidic environment. Plasmonic nanopipettes can be further developed to monitor other intracellular biomarkers.

Introduction

Reliable detection and quantitative analysis of biomarkers at a single-cell level are critical and vital for detecting diseases earlier and understanding the fundamental biological process better. Yet, a low concentration of biomarkers, micron dimensions (around 1–50 μm), and the dynamic nature of living cells make single-cell intracellular content analysis challenging with traditional analytical methods.[1,2] In the past several decades, several analytical techniques have emerged to overcome the challenges of single-cell intracellular sensing, including fluorescence-based spectroscopy[3]/microscopy,[4] dark-field scattering microscopy,[5] surface-enhanced Raman spectroscopy (SERS),[6] and nanopore/nanoelectrode sensing.[7] Fluorescence-based spectroscopy/microscopy techniques have been routinely used for single-cell analysis as they are capable of tracking intracellular molecules individually with high spatial and temporal resolution. However, only the limited number of cell-permeant fluorophores[8] can be selected or the gene construction technique[9] is required to allow intracellular sensing of live cells. Also, fluorophores have an intrinsic stability problem associated with photobleaching and blinking over long timescales.[10–12] SERS is an attractive alternative to fluorescence-based spectroscopy/microscopy techniques for biological sensing and has gained increasing attention.[13] The SERS signal is more photostable and provides multiple narrow bands at the same time, which allows for unparalleled multiplex detection. During biological sensing using the traditional SERS technique,[14,15] untethered plasmonic nanoparticles (NPs) enter a cell through endocytosis to enable intracellular SERS detection. The advantage of the untethered method is that it is convenient to use and less invasive to cells. However, the cellular retention time of NPs is typically long, and the intracellular distribution of these nanoprobes is uncontrollable.

To address the problems associated with the uncontrollable delivery of untethered NPs, a tethered substrate was used for "point-and-shoot" single-cell analysis. Tethered substrates include carbon nanotubes,[16,17] fiber-optic tips,[18] nanopipettes, nanoelectrodes,[19] and nanopores.[20,21] Glass micropipettes have been widely used in single ion channel measurements in electrophysiology. In recent years, nanopipettes with an apex size of a few hundred nanometers or less have been used for

[a]*Department of Physics, Florida International University, 11200 SW 8th St., Miami, FL 33199, USA. E-mail: jinhe@fiu.edu*
[b]*Department of Chemistry and Biochemistry, Florida International University, 11200 SW 8th St., Miami, FL 33199, USA*
[c]*Biomolecular Sciences Institute, Florida International University, 11200 SW 8th St., Miami, FL 33199, USA*

†Electronic supplementary information (ESI) available. See DOI: 10.1039/d0an00838a

intercellular measurements. Pourmand's group pioneered the nanopipette robotic 'nanobiopsy' system for single-cell genome sequencing.[22] Nanopipettes are also compatible with the traditional patch-clamp system. Flexible nanopipettes have been used to investigate *in vivo* cells or tissues with minimal cell damage.[23,24] Because of the advantages of SERS measurements, plasmonic nanopipettes have also been fabricated to enable SERS-based intracellular measurements.[25–30] Although promising, the development of plasmonic nanopipettes for intracellular applications is still at an early stage. For example, to generate enough SERS signals for sensing, the size of the tip of the plasmonic nanopipette should be generally bigger, which may cause greater cellular damage during the insertion of the plasmonic nanopipette tip. Therefore, to enable long-term time-resolved intracellular measurement, it is important to optimize both the nanopipette geometry and the plasmonic substrate structure to balance the needs for enhancing SERS signals and minimizing cell damage.

Herein, we developed a SERS-active nanopipette for intracellular pH (pH_i) sensing of individual eukaryotic cells. pH_i is an important parameter for regulating cellular function and behaviour and pathological conditions.[31] However, effective intracellular sensors are still limited.[32] To minimize the cellular damage during the insertion of the nanopipette, we reduced the nanopipette apex size to below 200 nm. The geometry of the nanopipette has also been optimized to increase its flexibility to better match the stiffness of a cell. By optimizing the distribution, density, and surface chemistry of the adsorbed AuNPs on the outer surface of the nanopipette, we obtained a uniform, stable, and reproducible SERS-active substrate with high enhancement of Raman intensity. 4-Mercaptobenzoic acid (4-MBA) was used as the probe molecule and the ratiometric intensity signal of the COO^- stretching vibration mode was calibrated for pH sensing. To evaluate the dynamic response of the nanopipette to pH changes in real time, the nanopipette was first tested in a controlled fluidic flow in a microfluidic device. Then, the nanopipette was used to study the pH_i change of individual live cells. By changing the extracellular pH (pH_e), we compared the cytoplasmic pH changes between cancer cells and normal cells.

Experimental

Reagents and materials

4-Mercaptobenzoic acid (4-MBA, 99%), (3-aminopropyl) triethoxysilane (APTES, >98%), sodium chloride (NaCl, >99%), potassium phosphate dibasic (K_2HPO_4), and potassium phosphate monobasic (KH_2PO_4) were purchased from Sigma-Aldrich. Phosphate buffered saline (PBS) powder (for pH 7.3–7.5), potassium chloride, absolute ethanol (200 proof), reagent alcohol (histology grade), hydrochloric acid (HCl, ~37%) and sodium hydroxide (NaOH) were purchased from Thermo Fisher Scientific. A citrate-protected 40 nm gold nanoparticle (AuNP) colloid was purchased from Ted Pella, Inc. All the aqueous solutions were prepared using deionized (DI) water (~18 M ohm, Ultra Purelab System, ELGA/Siemens).

The batch solution with pH ranging from 4.3 to 10.1 for nanopipette nanoprobe calibration was obtained by adding HCl or NaOH. The pH value ranging from 6.0 to 8.0 was obtained by changing the volume ratio of K_2HPO_4 and KH_2PO_4, as shown in Table ESI9.† The pH values were measured using a pH meter (SympHony SR60IC, VWR International).

Fabrication of pH-sensitive, SERS-active, and flexible nanopipettes

A borosilicate glass capillary with a filament (O.D.: 1.0 mm, I.D.: 0.58 mm, 15 cm length, Sutter Instrument Co.) was cleaned using piranha solution (**Caution**: Piranha solutions are highly corrosive and need to be handled with extreme caution!) for 30 min. Then, it was thoroughly rinsed both inside and outside using DI water and dried in an oven at 120 °C overnight. Glass long tapered (flexible) and short tapered (stiff) nanopipettes were prepared from the cleaned glass capillaries using a laser-based pipette puller (P-2000, Sutter Instrument) with different parameters. Parameters for long tapered nanopipettes: HEAT = 500, FIL = 4, VEL = 50, DEL = 255, and PUL = 100. Parameters for short tapered nanopipettes: HEAT = 400, FIL = 4, VEL = 50, DEL = 255, and PUL = 150.

The prepared glass nanopipettes were soaked in 0.4% (v/v) ethanol solution of (3-aminopropyl)triethoxysilane (APTES) for 1.5 h. After rinsing with ethanol, the nanopipettes were dried under an argon gas flow. Subsequently, APTES-modified nanopipettes were immersed in 150 pM AuNPs with a diameter of 40 nm for different times at 4 °C in a refrigerator. Finally, AuNP-loaded glass nanopipettes were soaked in ethanol solution with 1 mM 4-MBA for 1 h. After cleaning, the prepared nanopipettes were stored in 1× PBS before use.

Cell culture

HeLa cells and fibroblasts from mouse cells were cultured in Dulbecco's modified Eagle's medium (Gibco) with 10% fetal bovine serum, 5% CO_2 and 90% humidity at 37 °C. The cells were seeded on the cover slides (pre-modified with 0.01% poly-L-lysine to increase the cell adhesion). Before SERS measurement, the cells were gently washed two times with 1× PBS and the culture medium was supplied with K_2HPO_4/KH_2PO_4 buffer with different pH values. 4% paraformaldehyde was used to fix the live cells for 10 min and the cells were rinsed with 1× PBS.

SERS experiments

A micromanipulator (Thorlabs, PCS-5300) was used to control the position of the SERS-active nanopipette tip for single-cell measurements. SERS was performed on a home-built Raman microscopy setup (see details in ref. 33) using a Nikon inverted optical microscope. A 632.8 nm laser beam was focused on the nanopipette apex that was immersed in a liquid cell on the microscope sample stage. Neutral-density filters attenuated the laser power to 1 mW and the laser spot size was about 3 μm. Thus, the typical area intensity was about 35 μW μm^{-2}.

Time-resolved SERS spectra were collected with an acquisition time of 1–2 seconds per frame and accumulated 30 times for each spectrum. The spectral resolution was about 2 cm^{-1}.

Results and discussion

Fabrication and characterization of the flexible nanopipette-based nanoprobe

Nanopipettes have been successfully used in intracellular studies. However, the insertion of a nanopipette into small mammalian cells may damage the cell membrane.[34,35] With the aim of minimizing cellular damage, both the apex size and the stiffness of the nanopipette tip are optimized. In a recent report, a nanopipette showing minimized invasiveness in the intracellular measurement has a spring constant of 0.08 N m^{-1}.[23] Therefore, we prepared nanopipettes with a long tapered (shank length ~12.2 mm) geometry and a small tip diameter (sub-200 nm) using a pipette puller. Based on the classic beam theory, the spring constant of the nanopipette tip is estimated to be about 0.056 N m^{-1} with cantilever approximation (see details in ESI S1,†). In order to demonstrate the flexibility of the long tapered nanopipettes, the nanopipette tip is bent ~30° at a distance of ~3.4 mm from the apex and is then fully recovered after relaxing, as shown in Fig. 1A. The flexible tip can be repeatedly bent without breakage. In addition, the insertion of the flexible nanopipette tip into the living cells only induces minimal damage, which will be discussed in the single-cell intracellular pH sensing section. It demonstrates that flexible long tapered nanopipettes are preferable for intracellular measurements.

After fabrication, we modified the nanopipette tip to be a SERS-active substrate. The schematic diagram in Fig. 1B shows the steps to prepare a pH-sensitive and SERS-active nanopipette. The details are given in the Experimental section. Briefly, the tip of the nanopipette was first modified with APTES. Then, the nanopipette was soaked in an aqueous solution containing AuNPs for varying deposition times. Consequently, the outer surface of the nanopipette was coated with a layer of AuNPs through electrostatic force. Lastly, the nanopipette tip loaded with AuNPs were immersed in 4-MBA molecule solution to introduce a 4-MBA monolayer on the AuNPs.

The previous simulation results[36] have shown that the optimization of the SERS substrate can be achieved by controlling the AuNP coverage. We altered the AuNP deposition time to control the surface coverage of the AuNPs on the nanopipette tip while keeping the conditions of other steps the same. Fig. 1C shows the SEM images of the nanopipette tip after immersing the APTES-modified nanopipette in a colloidal AuNP solution for different time intervals. Before the depo-

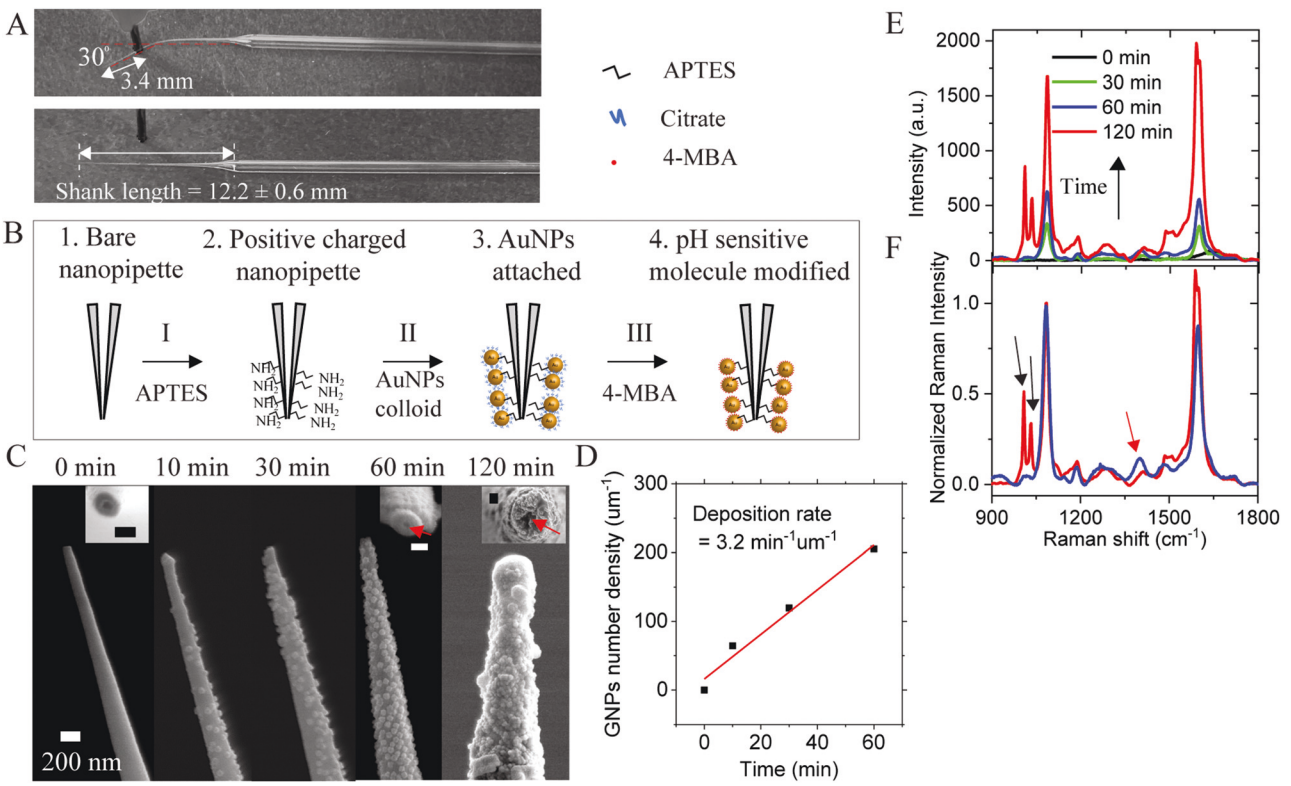

Fig. 1 (A) Optical images demonstrate the flexibility of a long tapered nanopipette tip. (B) Scheme of the procedures for the surface modification of a pH-sensitive nanopipette (not to scale). (C) SEM images of the nanopipette tip with different AuNP deposition times, ranging from 0 to 120 min. The insets show the top view of the nanopipette orifice. The scale bar is 100 nm in the inset images. (D) The AuNP number density at the tip (2 μm from the apex) as a function of the AuNP deposition time. (E) Typical Raman spectra of 4-MBA from the AuNP-loaded nanopipette tip after different AuNP deposition times. (F) Normalized Raman spectra of 4-MBA after 60 min (blue line) and 120 min (red line) of AuNP deposition time.

sition of AuNPs, the outer and inner diameters of the nanopipette are around 100 nm and 30 nm, respectively. After 60 min of deposition, the outer diameter of the nanopipette is increased to approximately 170 nm, revealing the adsorption of one sublayer of 40 nm AuNPs. The inner channel remains open, as indicated by the red arrow in Fig. 1C. After 120 min of deposition, the AuNP layer becomes much thicker with a multi-layer configuration. The inner diameter of the pore is also significantly reduced or even entirely blocked. Based on the SEM images, we can estimate the average number density of AuNPs on the nanopipette tip. As shown in Fig. 1D, the surface number density of AuNPs increases linearly at a rate of 3.2 min^{-1} μm^{-1} during the first 60 min of deposition. At 60 min, the surface number density of AuNPs is about 202 μm^{-2}.

After modifying the AuNP surface with 4-MBA molecules, Raman spectra of the tip of the AuNP-loaded nanopipette in 1× PBS were recorded. As shown in Fig. 1E, the overall 4-MBA Raman intensity increases with an increase in the number density of AuNPs at the tip. The nanopipette with a higher AuNP density possesses more plasmonic AuNPs and nanogaps, inducing higher electromagnetic enhancement of the SERS intensity. Fig. 1F shows the same Raman spectra of 4-MBA as in Fig. 1E normalized to the peak at 1077 cm^{-1}. The Raman spectra band at 1400 cm^{-1} (indicated by the red arrow) is used for pH sensing. This band will be further discussed in the next section. When the AuNP number density is too high (the red color spectrum), the intensity of this band decreases obviously along with the appearance of two new bands[37,38] near the peak at 1077 cm^{-1} (indicated by the black arrows). Thus, there is an optimal thickness for the AuNP layer. We determined that the thickness of the AuNP layer after 60 min of AuNP deposition is the best for pH sensing.

pH calibration of the flexible nanopipette-based nanoprobe

Fig. 2A shows the pH-sensing mechanism of 4-MBA molecules. The carboxyl group of 4-MBA is protonated at a lower pH and deprotonated at a higher pH, leading to changes in the Raman spectrum. Fig. 2B shows the pH-dependent Raman spectra of 4-MBA, collected from a fabricated pH-sensitive nanopipette. To avoid sample-to-sample variations, we used the ratiometric method to characterize the pH-dependent response of the SERS signal. Here, the band at 1077 cm^{-1}, from the stretching mode of C–S coupled with the benzene ring, is used as the internal reference. All other bands in the SERS spectra were normalized to the internal reference (all SERS spectra after this point were normalized, if not mentioned otherwise). The pH value of the bath solution varies from 4.3 to 10.1, resulting in the systematic changes in four major spectral regions, as marked with numbers (i) to (iv) in Fig. 2B.

Fig. 2C shows the zoomed-in view of the four pH-sensitive spectral regions. We assigned the Raman bands based on the literature[39–42] and our density functional theory (DFT) calculation (ESI S2,†). Fig. 2C(i) shows the bands at 688 and

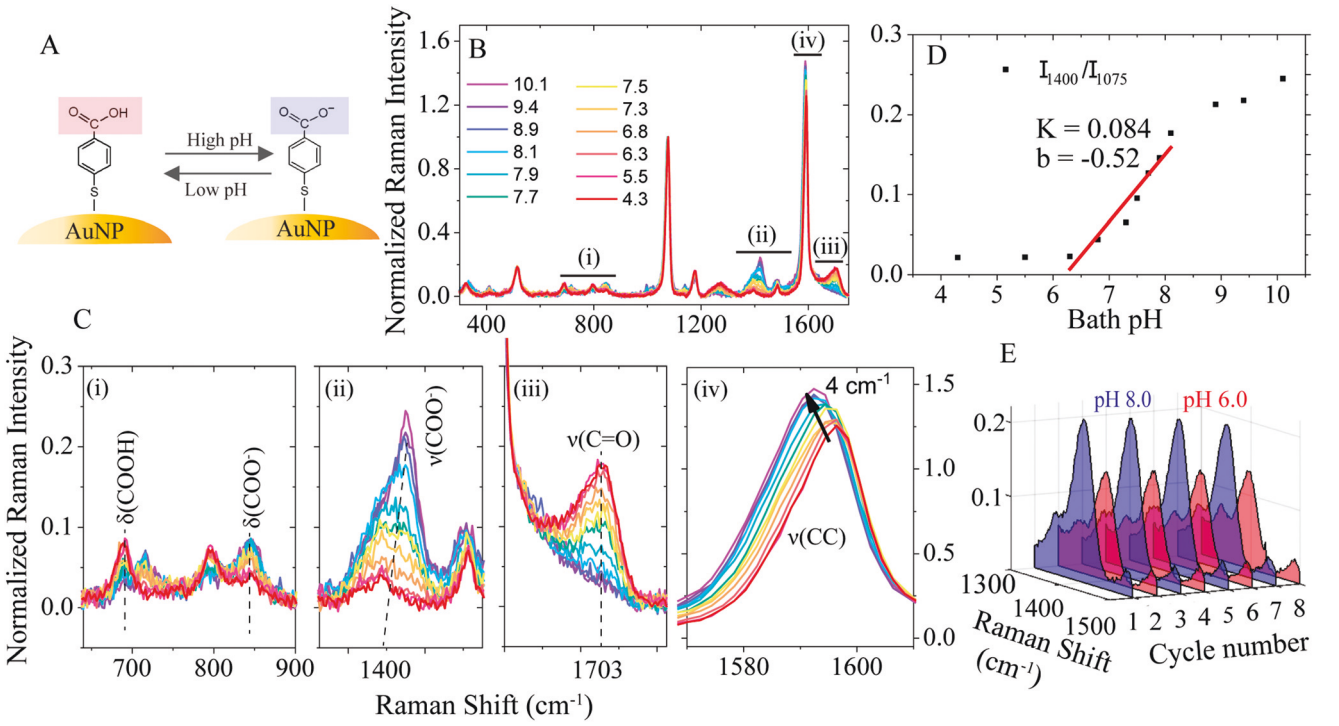

Fig. 2 (A) Schematic of reversible changes of the carboxyl group of 4-MBA as a result of pH changes. (B) SERS spectra of the nanopipette-based nanoprobe in bath solution with different pH values. (C) ((i)–(iv)) The zoomed-in view of four pH-sensitive spectral regions marked in (B). (D) pH calibration curve obtained by plotting the intensity ratio of 1400 cm^{-1} (I_{1400}/I_{1075}) against different pH values. The black dots are fitted by a linear regression equation and plotted as a solid red line. (E) The 3D SERS spectra of the normalized intensity change of the band at 1400 cm^{-1} when the bath solution pH was alternated between 8.0 and 6.0 for 8 cycles.

847 cm^{-1}, which are attributed to the bending mode of δ(COOH) and $\delta(COO^-)$. The two peaks decreased and increased concurrently with pH due to the deprotonation of –COOH, respectively. However, these bands were often overlapped with the bands from the glass substrate (see details in ESI Fig. S3†). Fig. 2C(ii) shows the pH-dependent change of the band at 1400 cm^{-1}, which is assigned to the symmetric COO– stretching mode ($\nu(COO^-)$). Its intensity increases with an increase in the solution pH. Fig. 2C(iii) shows the pH-dependent band at 1703 cm^{-1}, which is attributed to the stretching mode of the carbonyl group (ν(C═O)). Its intensity decreases with an increase in the solution pH. However, if the overall SERS intensity is weak, like in the case of intracellular measurement, the bending mode of water molecules at 1640 cm^{-1} may interfere with this mode (see ESI Fig. S3†). Fig. 2C(iv) shows the change in the band at 1592 cm^{-1}. The peak at 1592 cm^{-1} shows a 4 cm^{-1} wavenumber downshift, as the solution pH increases from 4.3 to 10.1, which is due to the breaking of symmetry upon the deprotonation of the carboxyl group.[30] However, this Raman shift is relatively small considering the 2 cm^{-1} spectral resolution of our setup.

All four regions can be used to detect local pH changes for different applications. Among them, we found that the band at 1400 cm^{-1} in Fig. 2C(ii) is the most robust and sensitive peak for the cellular application. Therefore, we used this band for the following experiments. Fig. 2D shows the plot of intensity ratio I_{1400}/I_{1077} *versus* bath solution pH, in which the most sensitive pH range is from 6.0 to 8.0. A linear fit to the data in this dynamic range gives a slope of 0.084. The noise level of the normalized intensity is about 0.015, which gives the pH sensitivity of 0.2 units. The measured slope values vary from 0.029 to 0.084 for different nanopipettes. Therefore, it is important to obtain the calibration curve for each nanopipette. The reproducibility of the nanopipette for pH sensing was also tested. Fig. 2E shows that the spectral changes of the normalized intensity of the $\nu(COO^-)$ mode between pH 6.0 (red color) and 8.0 (blue color) are reproducible.

Dynamic response of the nanopipette-based pH nanoprobe to pH changes

Motivated by the temporal dynamics of living cells, it is essential to understand the response time of the nanoprobe for dynamic pH changes in the solution. Fig. 3A shows the fluidic

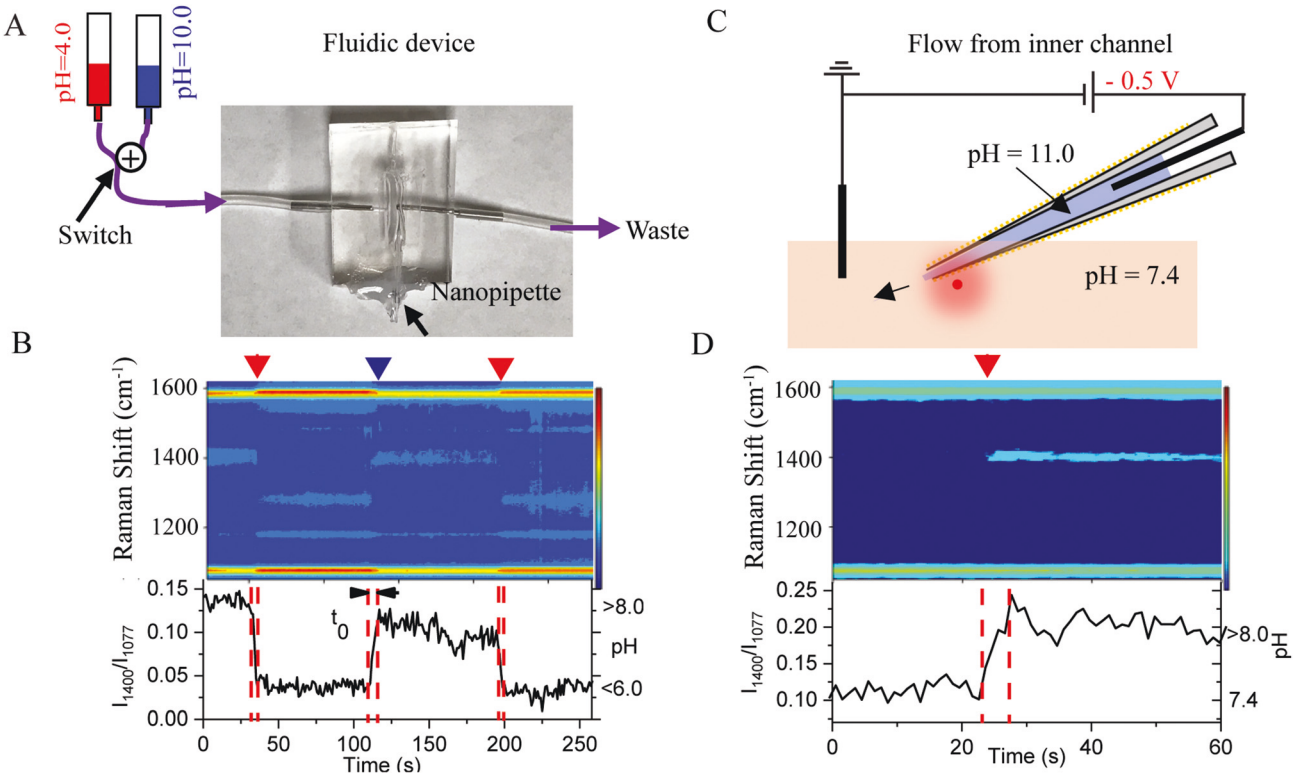

Fig. 3 (A) Schematic (not to scale) of a fluidic device with the embedded nanopipette-based nanoprobe. The bottom of the fluidic device is sealed with a cover glass. Solution with two different pH values passes through the nanopipette alternatively. (B) Top: Dynamic responding of SERS heatmap as two different pH bulk solutions pass through the nanopipette. Red and blue arrows indicate the moment that pH 4.0 and pH 10.0 bulk solution passing to the nanopipette. Bottom: Intensity ratio (I_{1400}/I_{1077}) time trace and right *y*-axis indicate the pH value. (C) Schematic of experimental setup (not to scale) to show the electrically control of local pH change using the nanopipette open channel. The nanopipette filled with pH 11 solution is placed in a bath solution of pH 7.4. (D) Top: Dynamic responding of SERS heatmap as H^+ exchange through the nanopipette open channel. The red arrow indicates the moment when –500 mV potential is applied. Bottom: Intensity ratio (I_{1400}/I_{1077}) time trace and right *y*-axis indicate the pH value using the calibration curve. The Raman spectra were acquired at a rate of 1 s per frame.

device made by polydimethylsiloxane (PDMS). The nanopipette is embedded in the middle of the fluidic chamber. By switching two solutions with pH 4 and 8 at the inlet, controllable pH changes are introduced in the fluidic chamber. The measured real-time SERS changes are shown in the heatmap trajectory in Fig. 3B. From the intensity (I_{1400}/I_{1077})-time trace at the bottom panel of Fig. 3B, it can be seen that it takes about 5 s (indicated as t_0 in Fig. 3B) to reach the maximum signal in responding to the solution pH change. This response time is mainly limited by the fluid flow speed. It takes about 5 s for the solution to fully fill the 1000 μL fluidic chamber with a speed of 200 μL s^{-1}, while the resolution time of the Raman signal is 1 s. Nevertheless, these results imply that the nanopipette-based pH nanoprobe has a pH response time at least of a few seconds.

The open channel of the nanopipette can also be utilized for pH sensing. A proof-of-concept experiment is shown in Fig. 3C. The pH of the solution inside the nanopipette barrel is 11 and the pH of the bath solution is 7.4. By applying a negative bias at the Ag/AgCl electrode inside the nanopipette barrel, the hydroxyl ions inside the nanopipette are driven out of the nanopipette barrel by the electric force. The effect of the bias-driven local pH change is shown in the SERS trajectory shown in Fig. 3D. At zero bias, the SERS trajectory was very stable and no spectral changes were detected (see ESI Fig. S4†). After applying −0.5 V, the peak at near 1400 cm^{-1} increased significantly, suggesting the increase in local pH. Therefore, the concentration gradient alone is not enough to drive hydroxyl ions out of the nanopipette tip. The applied bias is effective to deliver hydroxyl ions from the nanopipette tip to the bath solution. This experiment demonstrates that the SERS-active nanopipette loaded with molecules/ions inside the barrel could be used to electrically regulate the molecule/ion delivery while simultaneously monitoring the real-time and *in situ* changes induced by the delivered molecules/ions through Raman spectral changes.

Single-cell intracellular pH sensing

We further used the pH-sensitive nanopipette to detect pH_i changes in individual cells. Controlled using a piezo micromanipulator, the pH-sensitive nanopipette tip is inserted into HeLa and fibroblast cells at the center of the cells. Time-resolved SERS measurements are performed when the nanopipette tip reaches the designed location. Fig. 4A shows the optical images of HeLa cells when the nanopipette tip was approached to, inside, and retreated out of the cells, respectively. Similar optical microscopy images for the insertion process of the nanopipette in the fibroblast cells are shown in ESI Fig. S5.† The cell damage induced by the insertion of the nanopipette was tested by the trypan blue assay (see ESI S6†). After their insertion using a long tapered nanopipette, the cells appeared colorless within 60 min. In contrast, the cells inserted using a short tapered nanopipette often showed a distinctive blue color within 2 min. Thus, we were able to perform the live-cell experiments in an hour using the long tapered nanopipette. By using the nanopipette nanoprobe, the pH_i changes of HeLa and fibroblast cells in 1× PBS were measured based on the SERS spectra of 4-MBA molecules (results are shown in ESI Fig. S7†). Based on the calibration curve of each nanopipette, the measured pH_i values are always in the range between 7.1 and 7.5, which are typical for the healthy cells in the culture environment.

Then we measured the dynamic pH_i change induced by the change in pH_e. All the experiments were repeated at least three times with a good reproducibility. Fig. 4B shows a series of SERS spectra collected by the nanopipette tip inside the fixed (left) and live (right) fibroblast cells at different times. The pH_e of the medium was initially at 7.4 and replaced by pH_e 6.0 medium during 4–6 min. The acquisition of the Raman spectrum was interrupted for 2 min due to the solution exchange. Correspondingly, the magnitude of the peak at 1400 cm^{-1} in the SERS spectra is higher (in blue color) in the first 4 min and then decreases at 6 min (in red color) for both fixed and live fibroblast cells. However, at a later time, the peak height at 1400 cm^{-1} increases gradually for live fibroblast cells but not for the fixed fibroblast cells.

Based on the calibration curve, we plotted the pH_i change as a function of time for both cells in Fig. 4C. For the fixed fibroblast cells, the pH_i quickly decreases and remains near 6.1. This is attributed to the increased permeability of the cell membrane of the fixed cells. The pH_i of the live fibroblast cells also decreases immediately with the change in pH_e. However, the pH_i of the live fibroblast cells gradually returns to ~7.3 after about 10 min, while the cells were remained in the weak acidic medium with pH_e 6. We did not observe visible changes in the morphology of the fibroblast cells. Therefore, the fibroblast cells likely adapt to the environmental pH changes after 10 min. After this, the live fibroblast cells can maintain their cytoplasmic pH near neutral while they are still in a slightly acidic environment.

For comparison, we also studied the pH_i response of HeLa cells when they were exposed to the same weak acidic environment. This result is shown in the right panel in Fig. 4C. Similar to the results of live fibroblast cells, the pH_i of HeLa cells decreases within 2 min with the exposure to the weak acidic environment. This change is much faster than the reported time of more than 10 min.[19,43] We speculated that the seal between the cell membrane and nanopipette tip may be affected by the sudden change in pH_e and allows more protons to enter the cytoplasm, leading to the relatively fast decrease in pH_i.[44] However, the leakage must be very small and can be resealed quickly because the cells are still viable. Different from the live fibroblast cells, the pH_i of HeLa cells begins to increase right after the decrease and returns to the initial neutral value in about 6 min. The quick response and faster recovery of pH_i of the HeLa cells indicate that the cancer cells may better regulate their pH_i and adapt to the acidic environment. Although more experiments on different types of cancer cells are needed to further confirm this point, the result is consistent with the fact that tumor is often in an acidic microenvironment.[45,46]

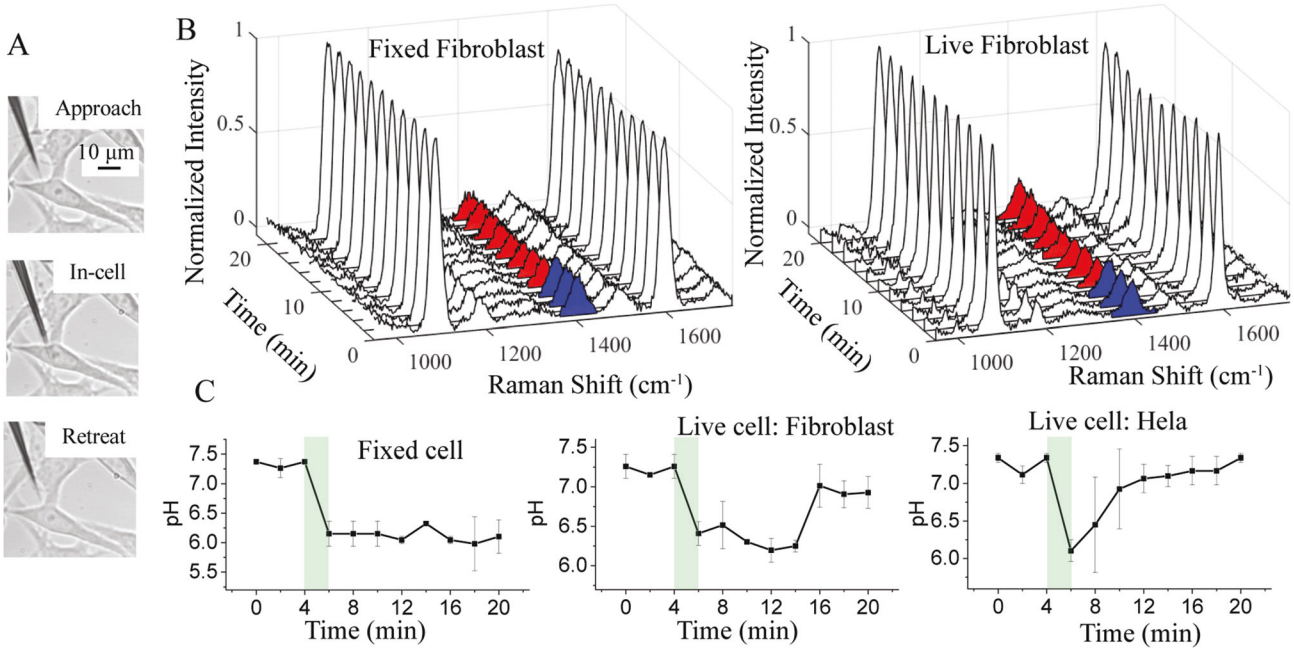

Fig. 4 (A) Bright-field images of HeLa cells before, during, and after the insertion of the nanopipette-based nanoprobe. (B) Normalized SERS spectra of the nanopipette-based nanoprobe in fixed and live fibroblast cells under pH_e = 7.4 (blue color filled 1400 cm^{-1}) and pH_e = 6.0 (red color filled 1400 cm^{-1}) stimulation for different time periods. (C) Variation of the pH_i value in fixed fibroblast cells, live fibroblast and HeLa cells *versus* time. The green-shaded regions highlight the solution exchange time when the pH_e is changed from 7.4 to 6.0. The error bars are obtained from the standard deviation of three separate measurements. The pH calibration curves for nanopipette nanoprobes are shown in ESI Fig. S9.†

Conclusions

In summary, we successfully prepared SERS-active flexible nanopipettes for live-cell intracellular pH sensing. Because of the nanoscale size of the apex and the long tapered geometry of the tip, the nanopipette is highly flexible and causes minimal cellular damage when it is inserted into the cell. The optimized AuNP surface distribution and density on the outer surface of the glass nanopipette enable sensitive and fast responses in the SERS signal of the pH reporter molecule 4-MBA. The pH response of the SERS nanoprobe is linear in the dynamic range between pH 6.0 and 8.0. The ratiometric SERS signal acquired from the nanopipette tip inside the cell is stable over time and the tip-to-tip variation is small. The non-specific adsorption of molecules and proteins on the AuNP surface only affects the overall Raman intensity but not the intensity ratio I_{1400}/I_{1077} of the 4-MBA molecule. We found that the cancerous HeLa cells could effectively regulate their pH_i and better adapt to the weakly acidic extracellular environment than normal cells, such as fibroblast cells.

The intracellular pH sensing performance of the developed SERS-active nanopipette is comparable with those of the commercially available fluorescent probes such as pHrodo Red and pHrodo Green in terms of sensitivity (~0.2 pH units) but has the advantages of high spatial resolution, long-term stability and multiplex detection. There are still a lot of rooms to improve this sensor. The shape and size of the AuNPs can be further optimized to improve the sensitivity. By introducing antifouling reagents, *e.g.*, polyethylene glycol (PEG), during chemical modification, the stability and selectivity of the sensor can also be improved. The pH reporter molecule 4-MBA can be replaced by or mixed with other molecules to expand the dynamic range of the pH sensing. This sensor can also be easily tailored to detect other biomarkers using different Raman probe molecules. The demonstrated on-demand local delivery is another advantage of this sensor. Therefore, we expect that plasmonic nanopipettes can be a promising sensor platform for varying single-cell analysis applications, especially real-time intracellular sensing.

Conflicts of interest

There are no conflicts to declare.

Acknowledgements

This work is supported by the Engineering Research Centers Program of the National Science Foundation under NSF Cooperative Agreement No. EEC-1647837 and NSF (CBET1454544). J. Guo thanks for the support provided by the Dissertation Year Fellowship award program. J. Moscoso acknowledges the REU support from the Science and Technology Center on Real-Time Functional Imaging, a National Science Foundation Science and Technology Center

(grant DMR 1548924). Y. Lai and Y. Liu are supported by the National Institute of Health grant NIHR01ES023569. We also acknowledge FIU AMERI for the use of the SEM.

Notes and references

1 P. Dittrich and N. Jakubowski, *Anal. Bioanal. Chem.*, 2014, **406**, 6957–6961.
2 G.-C. Yuan, L. Cai, M. Elowitz, T. Enver, G. Fan, G. Guo, R. Irizarry, P. Kharchenko, J. Kim, S. Orkin, J. Quackenbush, A. Saadatpour, T. Schroeder, R. Shivdasani and I. Tirosh, *Genome Biol.*, 2017, **18**, 84.
3 S. Weiss, *Science*, 1999, **283**, 1676–1683.
4 K. Okabe, N. Inada, C. Gota, Y. Harada, T. Funatsu and S. Uchiyama, *Nat. Commun.*, 2012, **3**, 705.
5 W. Qian, X. Huang, B. Kang and M. El-Sayed, *J. Biomed. Opt.*, 2010, **15**, 046025.
6 K. A. Willets, *Anal. Bioanal. Chem.*, 2009, **394**, 85–94.
7 Y.-L. Ying, Y.-X. Hu, R. Gao, R.-J. Yu, Z. Gu, L. P. Lee and Y.-T. Long, *J. Am. Chem. Soc.*, 2018, **140**, 5385–5392.
8 K. W. Teng, Y. Ishitsuka, P. Ren, Y. Youn, X. Deng, P. Ge, S. H. Lee, A. S. Belmont and P. R. Selvin, *eLife*, 2016, **5**, e20378.
9 J. Llopis, J. M. McCaffery, A. Miyawaki, M. G. Farquhar and R. Y. Tsien, *Proc. Natl. Acad. Sci. U. S. A.*, 1998, **95**, 6803–6808.
10 T. BERNAS, M. ZARĘBSKI, R. R. COOK and J. W. DOBRUCKI, *J. Microsc.*, 2004, **215**, 281–296.
11 A. Wright, W. A. Bubb, C. L. Hawkins and M. J. Davies, *Photochem. Photobiol.*, 2002, **76**, 35–46.
12 L. Song, R. P. M. van Gijlswijk, I. T. Young and H. J. Tanke, *Cytometry*, 1997, **27**, 213–223.
13 J. P. Nolan, E. Duggan, E. Liu, D. Condello, I. Dave and S. A. Stoner, *Methods*, 2012, **57**, 272–279.
14 K. Kneipp, A. S. Haka, H. Kneipp, K. Badizadegan, N. Yoshizawa, C. Boone, K. E. Shafer-Peltier, J. T. Motz, R. R. Dasari and M. S. Feld, *Appl. Spectrosc.*, 2002, **56**, 150–154.
15 I. R. Nabiev, H. Morjani and M. Manfait, *Eur. Biophys. J.*, 1991, **19**, 311–316.
16 J. J. Niu, M. G. Schrlau, G. Friedman and Y. Gogotsi, *Small*, 2011, **7**, 540–545.
17 R. Singhal, Z. Orynbayeva, R. V. Kalyana Sundaram, J. J. Niu, S. Bhattacharyya, E. A. Vitol, M. G. Schrlau, E. S. Papazoglou, G. Friedman and Y. Gogotsi, *Nat. Nanotechnol.*, 2010, **6**, 57.
18 J. P. Scaffidi, M. K. Gregas, V. Seewaldt and T. Vo-Dinh, *Anal. Bioanal. Chem.*, 2009, **393**, 1135–1141.
19 R. C. Thomas, *J. Physiol.*, 1974, **238**, 159–180.
20 R. E. Özel, A. Lohith, W. H. Mak and N. Pourmand, *RSC Adv.*, 2015, **5**, 52436–52443.
21 L. Hailing, J. Qiucen, P. Jie, J. Zeyu, C. Jiao, J. Lina, X. Xinghua and W. Kang, *Adv. Funct. Mater.*, 2018, **28**, 1703847.
22 P. Actis, M. M. Maalouf, H. J. Kim, A. Lohith, B. Vilozny, R. A. Seger and N. Pourmand, *ACS Nano*, 2014, **8**, 546–553.
23 K. Jayant, M. Wenzel, Y. Bando, J. P. Hamm, N. Mandriota, J. H. Rabinowitz, I. J.-L. Plante, J. S. Owen, O. Sahin, K. L. Shepard and R. Yuste, *Cell Rep.*, 2019, **26**, 266–278.e5.
24 W. Wang, F. Zhao, M. Li, C. Zhang, Y. Shao and Y. Tian, *Angew. Chem., Int. Ed.*, 2019, **58**, 5256–5260.
25 E. A. Vitol, Z. Orynbayeva, M. J. Bouchard, J. Azizkhan-Clifford, G. Friedman and Y. Gogotsi, *ACS Nano*, 2009, **3**, 3529–3536.
26 S. Hanif, H.-L. Liu, S. A. Ahmed, J.-M. Yang, Y. Zhou, J. Pang, L.-N. Ji, X.-H. Xia and K. Wang, *Anal. Chem.*, 2017, **89**, 9911–9917.
27 K. J. Freedman, C. R. Crick, P. Albella, A. Barik, A. P. Ivanov, S. A. Maier, S.-H. Oh and J. B. Edel, *ACS Photonics*, 2016, **3**, 1036–1044.
28 S. Hanif, H. Liu, M. Chen, P. Muhammad, Y. Zhou, J. Cao, S. A. Ahmed, J. Xu, X. Xia, H. Chen and K. Wang, *Anal. Chem.*, 2017, **89**, 2522–2530.
29 J.-F. Masson, J. Breault-Turcot, R. Faid, H.-P. Poirier-Richard, H. Yockell-Lelièvre, F. Lussier and J. P. Spatz, *Anal. Chem.*, 2014, **86**, 8998–9005.
30 H.-L. Liu, J. Cao, S. Hanif, C. Yuan, J. Pang, R. Levicky, X.-H. Xia and K. Wang, *Anal. Chem.*, 2017, **89**, 10407–10413.
31 J. R. Casey, S. Grinstein and J. Orlowski, *Nat. Rev. Mol. Cell Biol.*, 2010, **11**, 50–61.
32 J. Han and K. Burgess, *Chem. Rev.*, 2010, **110**, 2709–2728.
33 J. Guo, J. Pan, S. Chang, X. Wang, N. Kong, W. Yang and J. He, *Small*, 2018, **14**, 1704164.
34 I. Laffafian and M. B. Hallett, *Biophys. J.*, 1998, **75**, 2558–2563.
35 M. G. Schrlau, N. J. Dun and H. H. Bau, *ACS Nano*, 2009, **3**, 563–568.
36 D. M. Solís, J. M. Taboada, F. Obelleiro, L. M. Liz-Marzán and F. J. García de Abajo, *ACS Photonics*, 2017, **4**, 329–337.
37 T. Ma, J. Guo, S. Chang, X. Wang, J. Zhou, F. Liang and J. He, *Phys. Chem. Chem. Phys.*, 2019, **21**, 15940–15948.
38 Y. Zong, Q. Guo, M. Xu, Y. Yuan, R. Gu and J. Yao, *RSC Adv.*, 2014, **4**, 31810–31816.
39 S. Handa, Y. Yu and M. Futamata, *Vib. Spectrosc.*, 2014, **72**, 128–133.
40 H. T. Phan and A. J. Haes, *J. Phys. Chem. C*, 2018, **122**, 14846–14856.
41 G. Lu, B. Shrestha and A. J. Haes, *J. Phys. Chem. C*, 2016, **120**, 20759–20767.
42 S. B. Lee, K. Kim and M. S. Kim, *J. Raman Spectrosc.*, 1991, **22**, 811–817.
43 M. P. Fellenz and L. E. Gerweck, *Radiat. Res.*, 1988, **116**, 305–312.
44 M. I. Angelova, A.-F. Bitbol, M. Seigneuret, G. Staneva, A. Kodama, Y. Sakuma, T. Kawakatsu, M. Imai and N. Puff, *Biochim. Biophys. Acta, Biomembr.*, 2018, **1860**, 2042–2063.
45 Y. Kato, S. Ozawa, C. Miyamoto, Y. Maehata, A. Suzuki, T. Maeda and Y. Baba, *Cancer Cell Int.*, 2013, **13**, 89–89.
46 B. A. Webb, M. Chimenti, M. P. Jacobson and D. L. Barber, *Nat. Rev. Cancer*, 2011, **11**, 671–677.